Materials Advances

PAPER

Synthesis and characterization of all-inorganic (CsPbBr₃) perovskite single crystals†

Ramashanker Gupta, [abc] Ram Datt, [ad] Swapnil Barthwal, [c] Harshit Sharma, [ab] Animesh Pandey, [ab] Ridip Deka, [a] Pranjit Sarkar, [a] Sudhir Husale, [ab] Ritu Srivastava, *[ab] Vinay Gupta, *[e] Sandeep Arya [f] and Sandeep Pathak*[c]

This work investigates the synthesis of Cesium (Cs) based all-inorganic (CsPbBr₃) perovskite single crystals (PSCs) at low temperatures (45 °C) for application in photosensitive devices. The Cs-based PSCs are more environmentally stable in comparison with PSCs based on formamidinium and methylammonium. The crystals are grown using an inverse temperature crystallization method. The structural characterization was conducted using an X-ray diffractometer and confirms that the crystal is highly crystalline and it also shows that it belongs to the {110} family of planes. The optical analysis of the Cs-based single crystal was conducted using photoluminescence spectroscopy. The crystal has a bandgap of 2.18 eV as calculated by using the Tauc formula. Furthermore, a remarkable photocurrent analysis of the responsivity and detectivity parameters was conducted using a visible light laser (532 nm) and revealed values of ∼1 A W⁻¹ and 3.7 × 10¹¹ Jones, respectively. Thus, the all-inorganic PSC, CsPbBr₃, will be of benefit to optoelectronic device applications.

1 Introduction

Solution-processed metal halide perovskite materials have gained research interest around the globe after delivering promising results in perovskite solar cells (PSCs). PSCs have reached a power conversion efficiency of up to 25.8%.[1] Recently, single crystals based on perovskite materials have been proposed for use in optoelectronic devices. In the field of all-inorganic perovskite materials, the Cs-based perovskites always receive the most interest due to their higher ambient environmental stability.[2] Compared with the MA and FA cation, the degradation rate is lower in the ambient environment for Cs-based PSCs devices.[3–8] Formamidinium (FA) and methylammonium (MA) contain sensitive hydrocarbons that can easily be affected by humidity and oxygen-containing environments resulting in reduced ambient stability.[2,9] Replacing organic–inorganic (MA/FA) hybrid perovskites with all-inorganic Cs-based perovskites gives materials with superior mechanical properties and that are more moisture resistant.[6] The benefits of all-inorganic perovskite materials include higher carrier mobilities, longer diffusion lengths, low trap densities, and the direct bandgap of the materials.[10–12] These materials also show outstanding optical characteristics, for example, high quantum yields, high absorption coefficients, high luminous efficiencies, and easily tunable luminous wavelength.[13,14] These enormous potential benefits have astonishing results in the fields of high luminescence quantum dots (QD), stable solar cells, photodetectors, lasers, and high-energy photon detectors.[15–22] The growth of all-inorganic perovskite single crystals is significant for the exploration of their potential in single-crystalline-based optoelectronics devices.[23] Moreover, all-inorganic perovskite materials have reached new heights in solar cells and nanocrystal quantum dot applications.[18,24–29] CsPbBr₃ is a widely applied perovskite compound and is an all-inorganic perovskite material for use in solar cells and single crystal-based optoelectronic devices.[30–32] Detectors based on CsPbBr₃ are used in an extensive range of applications, such as high-energy radiation detection, medical diagnostics, environmental monitoring, security examinations, space science, *etc.*[4,33–37] High-energy photon detection requires a material with a large atomic number, to block the rays, a bandgap with a range between 1.5–3.0 eV, and high charge carrier mobilities.[38–42] In the case of CsPbBr₃, it is a semiconductor with a direct bandgap of 2.26 eV and has a high atomic number, thus implying that it has a high absorption radiation coefficient.[43,44] The trap densities in polycrystalline perovskite

[a] *Advanced Materials and Device Metrology, CSIR-National Physical Laboratory, Dr K. S. Krishnan Marg, New Delhi, 110012, India. E-mail: ritu@nplindia.org*

[b] *Academy of Scientific and Innovative Research (AcSIR), Ghaziabad, 201002, India*

[c] *Department of Energy Science and Engineering, Indian Institute of Technology Delhi, 110016, New Delhi, India. E-mail: sandeeppathak04@gmail.com*

[d] *SPECIFIC, Faculty of Science and Engineering, Swansea University, Bay Campus, Fabian Way, Swansea, SA1 8EN, UK*

[e] *Department of Physics, Khalifa University, Abu Dhabi, 127788, United Arab Emirates. E-mail: drvinaygupta@netscape.net*

[f] *Department of Physics, University of Jammu, Jammu, Jammu and Kashmir, 180006, India*

† Electronic supplementary information (ESI) available. See DOI: https://doi.org/10.1039/d2ma00345g

CsPbBr$_3$ are slightly higher than in single crystals.[2,45,46] Growth of perovskite single-crystals has been developed using different growth processes. In the past, the Bridgman method was employed to grow CsPbBr$_3$ single crystals and involves reacting CsBr and PbBr$_2$ in equimolar amounts at >600 °C, which is unsuitable for optoelectronics and cost-effective single-crystal synthesis.[47–52] Researchers have also applied the vertical Bridgman method for the synthesis of CsPbBr$_3$ large single crystals but, unfortunately, it also requires high temperature processing.[53] Thus, low-temperature solution-growth is an attractive method for perovskite single-crystal synthesis as this would be a low-cost method. Recently, the application of CsPbBr$_3$ single crystals as photodetectors has been of interest and it shows promising results in replacing conventional inorganic photodetectors.[54–56] Ding *et al.*[57] reported that CsPbBr$_3$ single crystals could be prepared by the antisolvent method, and their steady and transient performances delivered the highest responsivity of 0.028 A W^{-1}. Zhang *et al.*[58] prepared large-size CsPbBr$_3$ single crystals with low trap densities using a modified Bridgman method. The photoresponse measurements showed a high responsivity of 5.83 A W^{-1} when irradiated by a 532 nm laser. The synthesis of CsPbBr$_3$ single crystals has also been reported *via* a low-temperature processing method.[30,59] Ding *et al.*[57] reported the growth of CsPbBr$_3$ single crystals from saturated solution by dissolving CsBr and PbBr$_2$ in DMSO with continuous stirring at room-temperature and the highest responsivity was 0.028 A W^{-1}. Here we present the growth mechanism of all-inorganic perovskite single crystals using inverse temperature crystallization (ITC) at low temperature to open new avenues for the application of PSCs in optoelectronics devices alongside the benefit of synthesizing cost-effective single crystals. The ITC method grown CsPbBr$_3$ single crystal-based photodetector has been reported in the literature, nevertheless, it has shown low responsivity and detectivity.[6,30,60,61]

In the present work, we have demonstrated the synthesis of CsPbBr$_3$ single crystals using the ITC method and characterized this single crystal using UV-vis spectroscopy, photoluminescence spectroscopy, X-ray diffraction, and scanning electron microscopy (SEM).

2 Materials

The salts PbBr$_2$ (lead bromide) and CsBr (cesium bromide), as well as the dimethylsulfoxide (DMSO) solvent, were purchased from Sigma-Aldrich. All chemicals were used without any further purification.

3 Growth of CsPbBr$_3$ perovskite single crystal (PSCs)

In general, it is a three-step process, as shown in Fig. 1(a). The first step is preparation of the precursor solution and waiting for growth of the small seed crystals. In the second step, the best small crystal is selected. After that, in the final step, this small seed crystal is used to grow a much larger crystal by putting it into a new precursor solution. Fig. 1(b) shows a schematic illustration of the single-crystal growth process. First, we prepared an equimolar solution of CsBr and PbBr$_2$ in DMSO, stirring at 45 °C until we obtained a clear
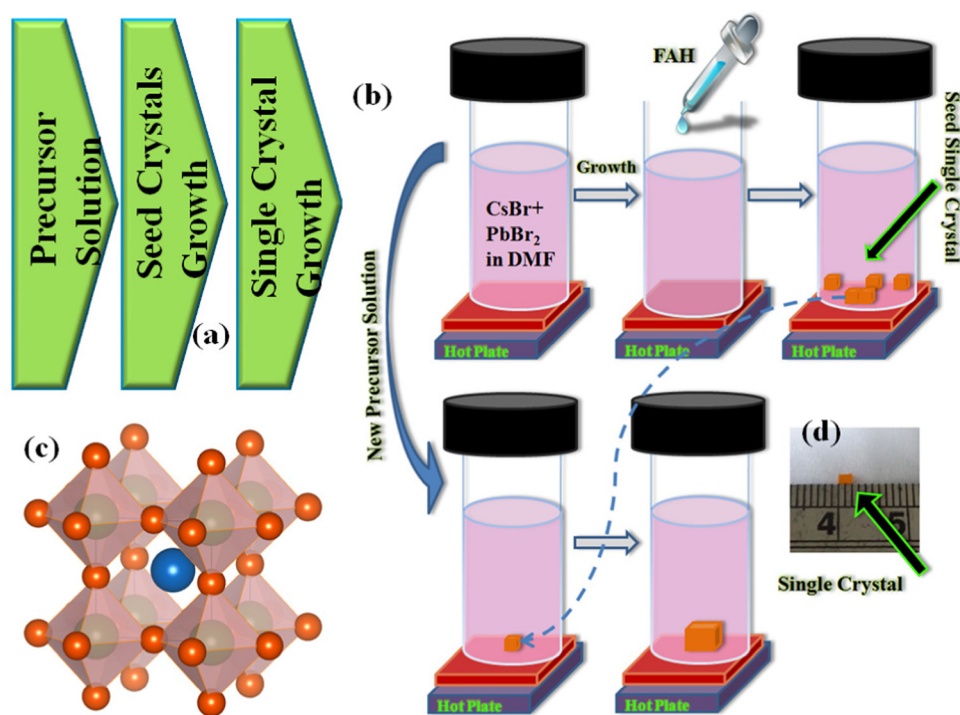

Fig. 1 (a) A block diagram of the single-crystal synthesis process, (b) step-by-step representation of the CsPbBr$_3$ PSCs synthesis, (c) perovskite structure, and (d) actual image of a CsPbBr$_3$ PSC.

solution. Next, we filtered the precursor solution over a PTFE filter and stored it in a new vial. We placed this vial without any disturbance in the silicon oil bath to grow the small single crystals. In the next step, we picked the best shaped small seed crystal, made a new precursor solution, and placed this seed at the bottom of the vial. Fig. 1(c and d) show the perovskite structure and the final $CsPbBr_3$ perovskite single crystal.

4 Characterization and measurements

The characterization was performed under ambient environmental conditions. In the structural characterization, a powder X-ray diffractometer (Rigaku Ultima IV Diffractometer: XRD) was used to analyze the $CsPbBr_3$ single crystal. The pattern was recorded at a speed of $8°$ min^{-1} and a step size of $0.02°$ using a copper Kα target. In the optical characterization, UV-vis (Perkin-Elmer Lambda 1050) and photoluminescence (Edinburgh FLS-980 d2d2) spectrometers were used for the absorption and photoluminescence studies, respectively.

5 Discussion

5.1 Photo-physical properties of the $CsPbBr_3$ perovskite single crystals

The photoluminescence and absorption properties of the synthesized PSCs are shown in Fig. 2(a and b), respectively.

The $CsPbBr_3$ single crystals show an emission peak at 565 nm, which is close to the value reported by Xu et al.[37] Also, the calculated band gap of the $CsPbBr_3$ single crystal is ~2.18 eV, which was calculated by using the Tauc relationship as shown in the inset of Fig. 2(b).

5.2 Structural characterization of the $CsPbBr_3$ perovskite single crystals

Fig. 2(c) shows the X-ray diffraction pattern of the $CsPbBr_3$ perovskite single crystal. The XRD peaks appear at angles with 2θ values of ~15.2°, ~30.6°, and ~47.1°, which denote the (110), (220), and (330) planes.[62] The planes show that the sample is crystalline in nature. This was also confirmed by the XRD analysis which shows a Cs-based single crystal that elongated along the {110} unit direction.

5.3 Solubility tests for the $CsPbBr_3$ perovskite single crystals

A solubility test was performed on the all-inorganic PSCs in their respective solution. First, a mortar and pestle were used to grind the $CsPbBr_3$ bulk single crystal. A small amount of $CsPbBr_3$ powder (0.01 g) was mixed in DMSO with continuous stirring and heated until a clear solution was obtained. The mass at the solution saturation point was marked as the maximum weight to be added to the vials. The exact process was then followed over the 20–100 °C temperature range within the same precursor solvent. For $CsPbBr_3$, ~40 °C is the
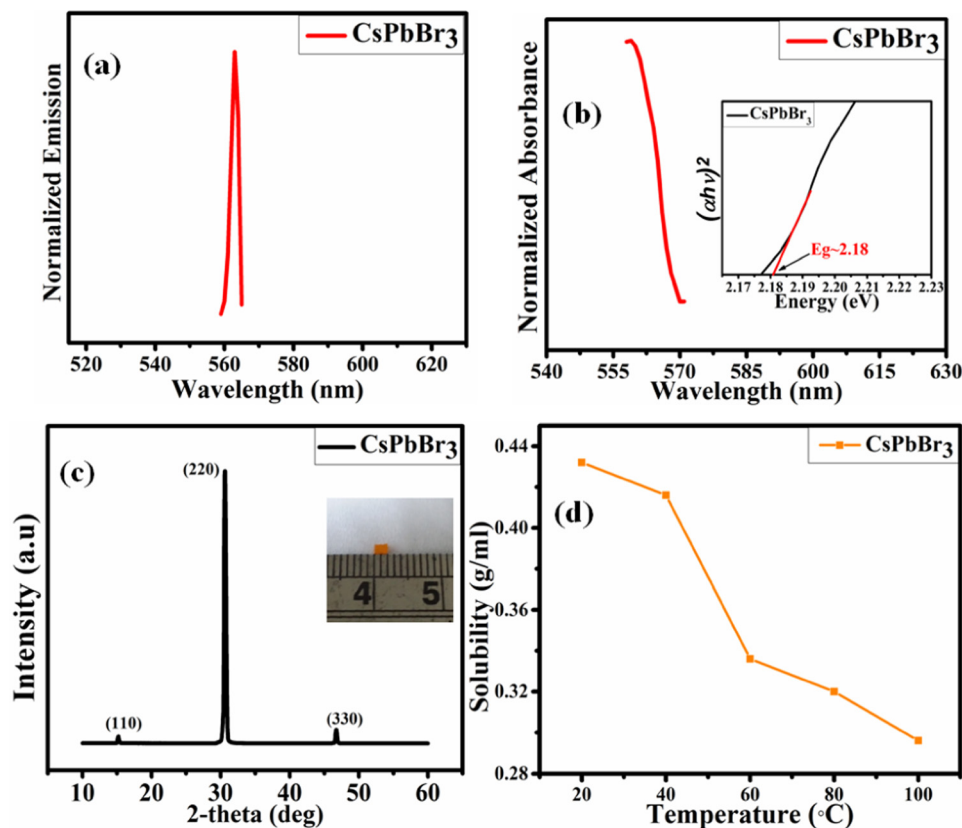

Fig. 2 (a) The $CsPbBr_3$ PSCs photoemission, and (b) absorption spectra (inset: Tauc plot). (c) The $CsPbBr_3$ crystal XRD pattern (inset: crystal image), and (d) the $CsPbBr_3$ crystal solubility test results.

maximum solubility temperature for crystallization, as shown in Fig. 2(d).

5.4 SEM and energy-dispersive X-ray analysis of the CsPbBr$_3$ PSCs

SEM was used to characterize the morphology of the synthesized crystal and the image is shown in Fig. S3 (ESI†). It shows that the single crystal surface was not smooth over the entire facet. Potential variation in the growth mechanism hindrance ions from attaching to other nearby ions to prevent the growth of a smooth shape. Thus, steps and flat surfaces are seen at the boundaries of the growing truncated single-crystal shapes. The elemental analysis using energy-dispersive X-ray spectroscopy is shown in Fig. S1 (ESI†), and the Pb and Cs content has been estimated to be a 1 : 1 ratio in CsPbBr$_3$.

5.5 CsPbBr$_3$ single-crystal photocurrent analysis

We studied the behavior of the grown PSCs under the illumination of different wavelengths of light. Ag (silver) paste was used for making the electrical contacts, as shown in Fig. 3(a). We also measured the I–V curve under irradiation of two different laser light wavelengths. It is observed that the photoconductivity of the CsPbBr$_3$ perovskite single-crystal gradually increases with irradiation power. It increases up to a few hundred nA compared to the experiments conducted in the dark, which showed single digit increases, as shown in Fig. 3(b).

5.6 Time-dependent photocurrent analysis for the CsPbBr$_3$ PSCs

The photocurrent analysis was conducted by illuminating the PSCs using the 376 nm and 532 nm wavelengths of two different types of laser. Fig. 3(c and d) show the time-dependent photocurrent of the CsPbBr$_3$ PSCs under three (2, 5, and 10 V) different applied voltages. After the incident light hit the single crystal, the photocurrent increased. A photocurrent of approximately 5 µA was achieved using the 532 nm laser (32 mW cm^{-2}) at a bias voltage of 10 V and the resultant curves are shown in Fig. 3(d). The photocurrent recovered rapidly after exposure to light illumination and it offers excellent repeatability, which promises photocurrent stability.[58] Fig. S2 (ESI†) shows the extended response under illumination with 376 nm light. The device performance was analyzed by calculating the responsivity, D^* (detectivity), rise time, and decay time parameters; the equations used for this are shown in the ESI.† The high detectivity and responsivity values found in response to visible light (532 nm) are 3.73×10^{11} Jones and ~ 1 A W^{-1}, respectively, as given in Table 1. Fig. 4(a) depicts the photocurrent response to both the lasers at 5 V. The CsPbBr$_3$ PSCs show a higher response to the 532 nm laser than to the 376 nm laser. As shown in Fig. 4(b), studies on the photocurrent output at different voltages have also been conducted for both lasers and both showed higher photocurrent at 10 V. Furthermore, the photocurrent vs responsivity graph, shown in Fig. 4(d), indicates a high responsivity value under illumination at 532 nm. Table 2 contains a summary of the transient photocurrent response of the CsPbBr$_3$ single crystal at different laser wavelengths and applied voltages. The responsivity of the CsPbBr$_3$ PSCs at different voltages and in response to both wavelength lasers is plotted in Fig. 4(e).
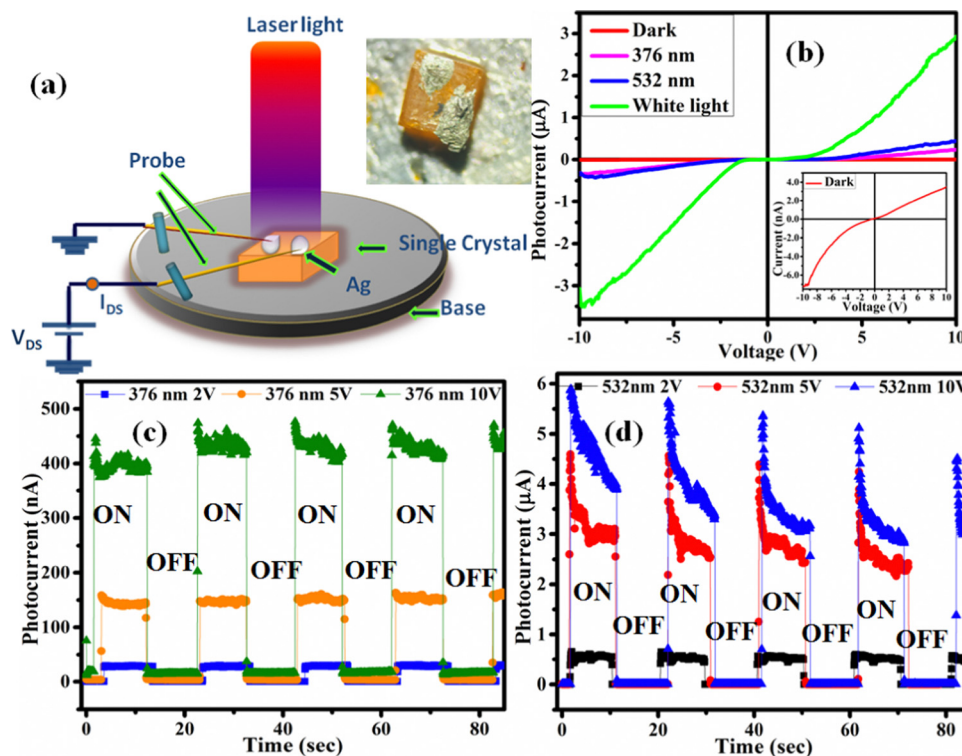

Fig. 3 (a) Illustration of the setup of the probe station (inset: cesium crystal image), and (b) the CsPbBr$_3$ single-crystal I−V curves. The rise and decay of the photocurrent of CsPbBr$_3$ single crystal, under (c) 376 nm, and (d) 532 nm laser illumination.

Table 1 Perovskite-based detectors and their photocurrent parameters

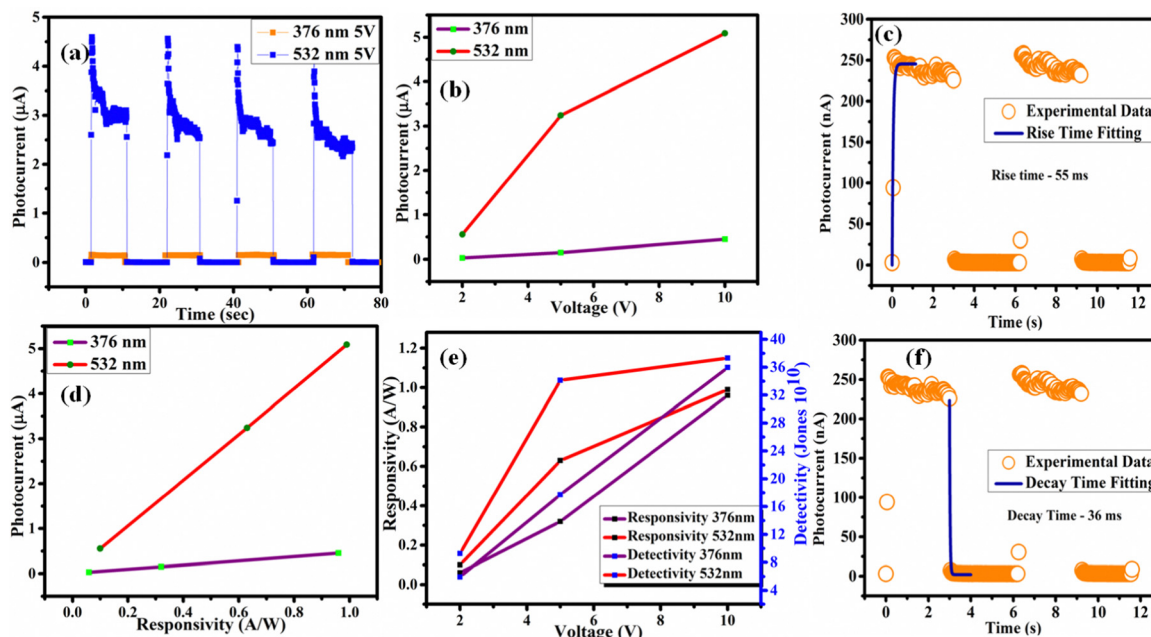| No.	Perovskite lead-based detector	Responsivity (A W^{-1})	Detectivity (Jones)	Rise time	Fall time	Ref.
(i)	$CsPbBr_3$	0.02	1.7×10^{11}			6
(ii)	$MAPbI_{2.5}Br_{0.5}$	~ 0.1	$\sim 4 \times 10^{12}$	<10 μs	<10 μs	63
(iii)	$MAPbI_xBr_{3-x}$	~ 0.01	—	2.3 s	2.7 s	64
(iv)	$MAPbCl_3$	~ 0.05	1.2×10^{10}	24 ms	62 ms	65
(v)	$CsPbBr_3$	0.028	1.8×10^{11}	<100 ms	<100 ms	57
(vi)	$CsPbBr_3$	~ 1.0	3.7×10^{11}	55 ms	36 ms	This work

Fig. 4 Photocurrent analysis in response to illumination with 376 and 532 nm wavelength lasers (a) fixed at 5 V, and (b) at different voltages. (c) Rise time experimental data and fitting. (d) Photocurrent *versus* responsivity and (e) responsivity *versus* voltage. (f) Fall time experimental data and fitting.

Table 2 Transient photocurrent response for CsPbBr$_3$ PSCs

Laser wavelength (nm)	Bias voltages (V)	Responsivity (A W^{-1})	Detectivity (Jones)
376	10	0.96	3.59×10^{11}
	5	0.32	1.77×10^{11}
	2	0.06	5.92×10^{10}
532	10	0.99	3.73×10^{11}
	5	0.63	3.41×10^{11}
	2	0.10	9.27×10^{10}

It shows that the responsivity of the CsPbBr$_3$ PSCs increases as the voltage also increase. Fig. 4(c and f) show the measured and fitted data for the rise time (55 ms) and decay time (36 ms), respectively. Compared with previous reports on the rise and decay time of CsPbBr$_3$ PSCs, both of the values obtained in our study are much faster. The short response times suggest that the material has low defect density and lower grain boundaries.

6 Conclusions

All-inorganic CsPbBr$_3$ perovskite single-crystals (PSCs) have the ability to work as photodetectors, like high energy photodetectors

for X-rays, Gamma rays, Beta rays, alpha rays, *etc.* This study describes the growth of high quality cesium-based all-inorganic perovskite single crystals under favorable low temperature and solution-processable conditions. A study of the crystallinity as well as the optical properties of the all-inorganic PSCs has been conducted. The XRD peaks at 2θ values of $\sim 15.2°$, $\sim 30.6°$, and $\sim 46.7°$ represent the (110), (220), and (330), planes, respectively. The existence of these planes confirms the highly crystalline nature of the material. Additionally, the XRD pattern confirmed that the crystal belongs to the {110} family of planes and showed that it was a single crystal. The peak photocurrent result for the PSCs was 5 μA reached under a 10 V applied bias voltage. The calculated detectivity and responsivity under illumination with a 532 nm laser were 3.71×10^{11} Jones and 1 A W^{-1}, respectively. This study has shown significant improvement in the detectivity and responsivity values of an all-inorganic perovskite-based single-crystal.

Author contributions

Ramashanker Gupta: investigation, methodology, conceptualization, writing – original draft; Ram Datt: writing – review &

editing, formal analysis; Swapnil Barthwal: methodology; Harshit Sharma: resources; Animesh Pandey: resources; Ridip Deka: resources; Pranjit Sarkar: resources; Sudhir Husale: resources; Ritu Srivastava: supervision; Vinay Gupta: supervision; Sandeep Arya: writing – review & editing; Sandeep Pathak: conceptualization, visualization, project administration.

Conflicts of interest

There are no conflicts to declare.

Acknowledgements

References

1 H. Min, D. Y. Lee, J. Kim, G. Kim, K. S. Lee, J. Kim, M. J. Paik, Y. K. Kim, K. S. Kim, M. G. Kim, T. J. Shin and S. Il Seok, *Nature*, 2021, **598**, 444–450.

2 L. Z. Jiaoxian Yu, A. G. Liu, C. Chen, Y. Li, M. Xu, T. Wang and G. Zhao, *J. Mater. Chem. C*, 2020, **8**, 6326.

3 J. Leroudier, J. Zaccaro, J. Debray, P. Segonds and A. Ibanez, *Cryst. Growth Des.*, 2013, **13**, 3613–3620.

4 Y. Feng, L. Pan, H. Wei, Y. Liu, Z. Ni, J. Zhao, P. N. Rudd, L. R. Cao and J. Huang, *J. Mater. Chem. C*, 2020, **8**, 11360–11368.

5 H. Zhao, Y. Fu, Z. Li, S. Yang, B. Xu, X. Liu, J. Xu, S. Liu and J. Yao, *J. Mater. Chem. A*, 2021, **9**, 4922–4932.

6 J. Ding, S. Du, Z. Zuo, Y. Zhao, H. Cui and X. Zhan, *J. Phys. Chem. C*, 2017, **121**, 4917–4923.

7 Y. Zhou and Y. Zhao, *Energy Environ. Sci.*, 2019, **12**, 1495–1511.

8 Q. Tai, K. Tang and F. Yan, *Energy Environ. Sci.*, 2019, **12**, 2375–2405.

9 X. Miao, T. Qiu, S. Zhang, H. Ma, Y. Hu, F. Bai and Z. Wu, *J. Mater. Chem. C*, 2017, **5**, 4931–4939.

10 D. Shi, V. Adinolfi, R. Comin, M. Yuan, E. Alarousu, A. Buin, Y. Chen, S. Hoogland, A. Rothenberger, K. Katsiev, Y. Losovyj, X. Zhang, P. A. Dowben, O. F. Mohammed, E. H. Sargent and O. M. Bakr, *Science*, 2015, **347**, 519–522.

11 Y. Fang, Q. Dong, Y. Shao, Y. Yuan and J. Huang, *Nat. Photonics*, 2015, **9**, 679–686.

12 M. I. Saidaminov, A. L. Abdelhady, B. Murali, E. Alarousu, V. M. Burlakov, W. Peng, I. Dursun, L. Wang, Y. He, G. MacUlan, A. Goriely, T. Wu, O. F. Mohammed and O. M. Bakr, *Nat. Commun.*, 2015, **6**, 1–6.

13 J. H. Kim, P. W. Liang, S. T. Williams, N. Cho, C. C. Chueh, M. S. Glaz, D. S. Ginger and A. K. Y. Jen, *Adv. Mater.*, 2015, **27**, 695–701.

14 G. Tong, L. K. Ono and Y. Qi, *Energy Technol.*, 2020, **1900961**, 1–17.

15 Y. Wei and J. Lin, *Chem. Soc. Rev.*, 2019, **48**, 310.

16 X. Sheng, G. Chen, C. Wang, W. Wang, J. Hui, Q. Zhang, K. Yu, W. Wei, M. Yi, M. Zhang, Y. Deng, P. Wang, X. Xu, Z. Dai, J. Bao and X. Wang, *Adv. Funct. Mater.*, 2018, **28**, 1–9.

17 Q. Zhang and Y. Yin, *ACS Cent. Sci.*, 2018, **4**, 668–679.

18 L. Gao and Q. Yan, *Sol. RRL*, 2019, **1900210**, 1–12.

19 X. Cheng, S. Yang, B. Cao, X. Tao and Z. Chen, *Adv. Funct. Mater.*, 2020, **1905021**, 1–20.

20 D. Ghosh, M. Y. Ali, D. K. Chaudhary and S. Bhattacharyya, *Sol. Energy Mater. Sol. Cells*, 2018, **185**, 28–35.

21 W. Liu, Z. Jiang, W. Fan, Q. Zhang and X. W. Sun, *J. Phys. Chem. Lett.*, 2021, **12**, 10197–10203.

22 Y. Hua, F. Cui, P. Zhang, G. Zhang, Q. Zhang and X. Tao, *Z. Anorg. Allg. Chem.*, 2022, **e202200025**, 1–7.

23 S. Arya, P. Mahajan, R. Gupta, R. Srivastava, N. Kumar Tailor, S. Satapathi, R. R. Sumathi, R. Datt and V. Gupta, *Prog. Solid State Chem.*, 2020, **60**, 100286.

24 M. Zhang, Z. Zheng, Q. Fu, Z. Chen, J. He, S. Zhang, L. Yan, Y. Hu and W. Luo, *CrystEngComm*, 2017, **19**, 6797–6803.

25 Y. Fu, H. Zhu, C. C. Stoumpos, Q. Ding, J. Wang, M. G. Kanatzidis, X. Zhu and S. Jin, *ACS Nano*, 2016, **10**, 7963–7972.

26 J. Li, H. Zhang, S. Wang, D. Long, M. Li, D. Wang and T. Zhang, *Materials*, 2018, **11**, 1–9.

27 Q. Fu, X. Tang, B. Huang, T. Hu, L. Tan, L. Chen and Y. Chen, *Adv. Sci.*, 2018, **5**, 1700387.

28 S. W. Eaton, M. Lai, N. A. Gibson, A. B. Wong, L. Dou, J. Ma, L. W. Wang, S. R. Leone and P. Yang, *Proc. Natl. Acad. Sci. U. S. A.*, 2016, **113**, 1993–1998.

29 S. Wei, Y. Yang, X. Kang, L. Wang, L. Huang and D. Pan, *Chem. Commun.*, 2016, **52**, 7265–7268.

30 Y. Rakita, N. Kedem, S. Gupta, A. Sadhanala, V. Kalchenko, M. L. Böhm, M. Kulbak, R. H. Friend, D. Cahen and G. Hodes, *Cryst. Growth Des.*, 2016, **16**, 5717–5725.

31 J. Song, Q. Cui, J. Li, J. Xu, Y. Wang, L. Xu, J. Xue, Y. Dong, T. Tian, H. Sun and H. Zeng, *Adv. Opt. Mater.*, 2017, **5**, 1–8.

32 Y. Gao, Y. Wu, H. Lu, C. Chen, Y. Liu, X. Bai, L. Yang, W. W. Yu, Q. Dai and Y. Zhang, *Nano Energy*, 2019, **59**, 517–526.

33 J. Peng, C. Q. Xia, Y. Xu, R. Li, L. Cui, J. K. Clegg, L. M. Herz, M. B. Johnston and Q. Lin, *Nat. Commun.*, 2021, **12**, 1531.

34 Z. Fan, J. Liu, W. Zuo, G. Liu, X. He, K. Luo, Q. Ye and C. Liao, *Phys. Status Solidi*, 2020, **217**, 2000104.

35 L. Pan, Y. Feng, P. Kandlakunta, J. Huang and L. R. Cao, *IEEE Trans. Nucl. Sci.*, 2020, **67**, 443–449.

36 Y. Zhong, K. Liao, W. Du, J. Zhu, Q. Shang, F. Zhou, X. Wu, X. Sui, J. Shi, S. Yue, Q. Wang, Y. Zhang, Q. Zhang, X. Hu and X. Liu, *ACS Nano*, 2020, **14**, 15605–15615.

37 Q. Xu, X. Wang, H. Zhang, W. Shao, J. Nie, Y. Guo, J. Wang and X. Ouyang, *ACS Appl. Electron. Mater.*, 2020, **2**, 879–884.

38 Y. Zhou, J. Chen, O. M. Bakr and O. F. Mohammed, *ACS Energy Lett.*, 2021, **6**, 739–768.

39 H. Wu, Y. Ge, G. Niu and J. Tang, *Matter*, 2021, **4**, 144–163.

40 G. J. Matt, I. Levchuk, J. Knüttel, J. Dallmann, A. Osvet, M. Sytnyk, X. Tang, J. Elia, R. Hock, W. Heiss and C. J. Brabec, *Adv. Mater. Interfaces*, 2020, **7**, 1901575.

41 L. Pan, Y. Feng, J. Huang and L. R. Cao, *IEEE Trans. Nucl. Sci.*, 2020, **67**, 2255–2262.

42 D. N. Dirin, I. Cherniukh, S. Yakunin, Y. Shynkarenko and M. V. Kovalenko, *Chem. Mater.*, 2016, **28**, 8470–8474.

43 M. Zhang, Z. Zheng, Q. Fu, Z. Chen, J. He, S. Zhang, C. Chen and W. Luo, *J. Cryst. Growth*, 2018, **484**, 37–42.

44 C. A. López, C. Abia, M. C. Alvarez-Galván, B. K. Hong, M. V. Martínez-Huerta, F. Serrano-Sánchez, F. Carrascoso, A. Castellanos-Gómez, M. T. Fernández-Díaz and J. A. Alonso, *ACS Omega*, 2020, **5**, 5931–5938.

45 D. Liu, L. Wu, C. Li, S. Ren, J. Zhang, W. Li and L. Feng, *ACS Appl. Mater. Interfaces*, 2015, **7**, 16330–16337.

46 Q. Han, S. H. Bae, P. Sun, Y. T. Hsieh, Y. Yang, Y. S. Rim, H. Zhao, Q. Chen, W. Shi, G. Li and Y. Yeng, *Adv. Mater.*, 2016, **28**, 2253–2258.

47 C. C. Stoumpos, C. D. Malliakas, J. A. Peters, Z. Liu, M. Sebastian, J. Im, T. C. Chasapis, A. C. Wibowo, D. Y. Chung, A. J. Freeman, B. W. Wessels and M. G. Kanatzidis, *Cryst. Growth Des.*, 2013, **13**, 2722–2727.

48 M. Sebastian, J. A. Peters, C. C. Stoumpos, J. Im, S. S. Kostina, Z. Liu, M. G. Kanatzidis, A. J. Freeman and B. W. Wessels, *Phys. Rev. B: Condens. Matter Mater. Phys.*, 2015, **92**, 235210.

49 D. J. Clark, C. C. Stoumpos, F. O. Saouma, M. G. Kanatzidis and J. I. Jang, *Phys. Rev. B: Condens. Matter Mater. Phys.*, 2016, **93**, 195202.

50 Y. He, Z. Liu, K. M. McCall, W. Lin, D. Y. Chung, B. W. Wessels and M. G. Kanatzidis, *Nucl. Instrum. Methods Phys. Res., Sect. A*, 2019, **922**, 217–221.

51 X. Chen, Y. Wang, J. Song, X. Li, J. Xu, H. Zeng and H. Sun, *J. Phys. Chem. C*, 2019, **123**, 10564–10570.

52 D. Kim, H. Ryu, S. Y. Lim, K. M. McCall, J. Park, S. Kim, T. J. Kim, J. Kim, Y. S. Kim, M. G. Kanatzidis, H. Cheong and J. I. Jang, *Chem. Mater.*, 2021, **33**, 7185–7193.

53 P. Zhang, Q. Sun, Y. Xu, X. Li, L. Liu, G. Zhang and X. Tao, *Cryst. Growth Des.*, 2020, **20**, 2424–2431.

54 J.-H. Cha, J. H. Han, W. Yin, C. Park, Y. Park, T. K. Ahn, J. H. Cho and D.-Y. Jung, *J. Phys. Chem. Lett.*, 2017, **8**, 565–570.

55 J. Liu, S. Cristoloveanu and J. Wan, *Phys. Status Solidi*, 2021, **218**, 2000751.

56 Y. Ren and V. Van, in *2019 24th OptoElectronics and Communications Conference (OECC) and 2019 International Conference on Photonics in Switching and Computing (PSC)*, 2019, pp. 1–3.

57 J. Ding, S. Du, Z. Zuo, Y. Zhao, H. Cui and X. Zhan, *J. Phys. Chem. C*, 2017, **121**, 4917–4923.

58 P. Zhang, G. Zhang, L. Liu, D. Ju, L. Zhang, K. Cheng and X. Tao, *J. Phys. Chem. Lett.*, 2018, **9**, 5040–5046.

59 Y. Cheng, M. Zhu, F. Wang, R. Bai, J. Yao, W. Jie and Y. Xu, *J. Mater. Chem. A*, 2021, **9**, 27718–27726.

60 R. Gupta, T. B. Korukonda, S. K. Gupta, B. P. Dhamaniya, P. Chhillar, R. Datt, P. Vashishtha, G. Gupta, V. Gupta, R. Srivastava and S. Pathak, *J. Cryst. Growth*, 2020, **537**, 125598.

61 R. Gupta, V. Gupta, R. Datt, S. Arya, A. Pandey, A. Singh, S. Husale, R. Srivastava and S. Pathak, *Mater. Adv.*, 2022, **3**, 2089–2095.

62 V. I. Yudin, M. S. Lozhkin, A. V. Shurukhina, A. V. Emeline and Y. V. Kapitonov, *J. Phys. Chem. C*, 2019, **123**, 21130–21134.

63 D. Arquer, X. Gong, R. P. Sabatini, M. Liu, G. Kim, B. R. Sutherland, O. Voznyy, J. Xu, Y. Pang, S. Hoogland, D. Sinton and E. Sargent, *Nat. Commun.*, 2017, **8**, 14757.

64 M. Cao, J. Tian, Z. Cai, L. Peng, L. Yang and D. Wei, *Appl. Phys. Lett.*, 2016, **109**, 233303.

65 G. Maculan, A. D. Sheikh, A. L. Abdelhady, M. I. Saidaminov, A. Haque, B. Murali, E. Alarousu, O. F. Mohammed, T. Wu and O. M. Bakr, *J. Phys. Chem. Lett.*, 2015, **6**, 3781–3787.